Bulletin of the Mineral Research and Exploration

http://bulletin.mta.gov.tr



The relationship between seismic quality factor and peak ground acceleration, a case study: M=4.3, 17.01.2015 Eskişehir Earthquake

Muammer TÜN[a]*

[a]*Eskişehir Technical University, Institute of Earth and Space Sciences, Department of Earth Sciences and Earthquake Engineering, Eskişehir, Turkey*

Research Article

Keywords:
Quality Seismic Factor, EstuNet Seismic Network, Strong Ground Motion, Peak Ground Acceleration, Eskişehir Graben.

ABSTRACT

Seismic wave propagation in subsurface media endures from absorption, which can be evaluated by the seismic quality factor Q (Q-factor). Absorption is frequency-dependent. Lower frequencies are absorbed less, while higher frequencies are absorbed more. Therefore, the Q Factor should be determined in the frequency domain. Q-factor is determined by the slope of the natural logarithm of the output-input signals ratio. Surface waves (Rayleigh and Love waves) are particularly important, as they are the more destructive phases of an earthquake. This study was focused on the Q-factor computation of the surface waves and demonstrated that the determination of the Q-factor is not affected from the dispersive properties of the surface waves. Data were obtained from surface wave signals of earthquake recorded at Eskişehir Technical University Seismic Network - EstuNet. The obtained Q-factor values represent the average values of the rocks that the waves cross between the input and output stations. Finally, the Q-factor map to the Peak Ground Acceleration (PGA) map using the M=4.3, 17.01.2015 Eskişehir earthquake data was compared. These records, show the arrival time of the earthquake from the epicenter to the stations of the seismic waves, and the peak ground acceleration values. In this study, local site effects of EstuNet accelerometric stations have been calculated by using the Standard Spectral Ratio (SSR) method. It is concluded that an inverse relationship exists between the computed Q-factor and measured PGA values. Therefore, the sites where the Q factor is very low should be analyzed in more detail in ground-based earthquake risk assessments.

Received Date: 30.08.2020
Accepted Date: 11.12.2020

1. Introduction

Seismic quality factor (Q-factor) studies date back to the early 1940s (Ricker, 1940). Since then, many researchers have studied the attenuation properties of earth substance (Johnston et al., 1979; Jongmans, 1990; Moya and Irikura, 2003; Raghukanth and Nadh Somala, 2009; Naresh et al., 2019) both in the field and in the laboratory. In-situ Q measurements are of interest in engineering geophysics. Absorption is usually measured by the inverse of the dimensionless Q. Amplitude is affected by energy loss due to anelastic processes or internal friction during wave propagation. This intrinsic attenuation may be distinguished from scattering attenuation. The strength of intrinsic attenuation is given by Q in terms of the fractional energy loss per cycle. Q is sometimes called the quality factor (Shearer, 2009; Stein and Wysession, 2009) and is inversely related to the strength of attenuation; low-Q regions are more attenuating than

Citation Info: Tün, M. 2021. The relationship between seismic quality factor and peak ground acceleration, a case study: M=4.3, 17.01.2015 Eskişehir Earthquake. The Bulletin of the Mineral Research and Exploration 166, 127-144. https://doi.org/10.19111/bulletinofmre.841785

**Corresponding author: Muammer TÜN, mtun@eskisehir.edu.tr*

high-Q regions. Seismic wave/soil (subsurface layers) interactions and responses are caused reflectors, refractors, or diffractors. Spherical divergence or absorption always exist as seismic waves propagate. These effects concurrently affect seismic waves as they travel. In this study, continuous factors that affect seismic waves were considered.

Attention of seismic waves has been measured for many years (Anderson and Archambeau, 1964; Anderson and Hart, 1978; Anderson and Kovach, 1964; Jackson and Anderson, 1970). The resultant distribution of attenuation versus depth (usually expressed by the dimensionless quality factor Q) is an important source of information in the earth's interior (Press, 1964). Accurate estimation of the Q factor is of great importance for the resolution enhancement of seismic data. Estimates of the quality, Q, factor are commonly obtained from vertical seismic data or stacked surface seismic data (Zhang and Ulrych, 2002; Li et al., 2016). This paper describes a method that Q-factor can be measured from the recording of strong ground motion.

The Q-factor provides valuable information on the physical properties of soil. A low Q-factor indicates the presence of an absorptive medium; absorption is frequency-dependent. Moreover, the effect of absorption becomes more prominent at higher frequencies (Gurevich and Pevzner, 2015). Some of the mechanical energy of a seismic wave is transferred to an irreversible dislocation and deformation within the rocks, producing friction and heat. Rock types, formation of fissures, cracks within the rocks, fault zones, liquefaction (migration of fluids in cracks and pores), landslides, and a change in water table level are the major indicators of absorption with low Q values. In the case of elastic behavior, after the passage of seismic waves, vibrating particles assume their original position. Elastic behavior causes minimum earthquake damage. In the case of anelastic, or plastic behavior, after the passage of seismic waves, vibrating particles cannot assume their original equilibrium position. Anelastic behavior causes maximum earthquake damage (Luzi et al., 2019; Mayoral et al., 2019; Miyakoshi et al., 2019).

The frequency dependent attenuation (Q) value which gives Quality factor (Q_0) of S-waves of the Punjab basin and this study is important to develop the ground motion model and simulations for seismic hazard studies (Naresh et al., 2019). Quality factor and site amplification are derived from the strong-motion data. The Quality factor represents a part of the total attenuation of Fourier spectral amplitudes reaching the ground surface (Raghukanth and Nadh Somala, 2009). Two strong motion networks, K-NET and KiKnet, recorded the aftershocks of the 2000 Tottori, Japan, earthquake. The results suggest that the study area presents a low Q value and that there is also amplification at borehole sites (Moya and Irikura, 2003).

The earthquake data from years 1900–2019 were downloaded from the KOERI (Kandilli Observatory and Earthquake Research Institute) web portal (http://www.koeri.boun.edu.tr/sismo/zeqdb/). During downloading, all the parameters were selected as accurately as possible with coordinated boundaries to cover Eskişehir Province for earthquakes with magnitudes greater than 3. The downloaded data was in .txt format, so it was first organized in Excel and then reformatted to .xls format so that it could be opened in ArcGIS. There were 161 earthquakes in total with magnitudes of greater than 3 that occurred within the study area within the selected date range. The result of the analysis shows that most of the earthquakes with magnitudes between 3 and 6.4 occurred in the southern part of Tepebaşı District and the northern part of Odunpazarı District. The earthquake occurrence is attributed to faults, because most of the earthquake epicenters are distributed between active faults. The 3499 houses, 10 schools, 15 mosques, and 3 official buildings were demolished, along with 1303 barns and haystacks in that earthquake in Eskişehir city center in the 20 February 1956 (Ms 6.4) Eskişehir earthquake. One person died (Ersoy, 1956). In the 17 August 1999 Kocaeli earthquake (Mw 7.4), which was approximately 250 km from Eskişehir city center, 86 people lost their lives in the city of Eskişehir, and 95 people were injured. Also, 70 houses/workplaces suffered severe damage, one building collapsed during the earthquake, and four buildings collapsed after the earthquake (Özmen, 2000).

The aim of this study is to show that the Q-factor can be measured from the recording of strong ground motion and to examine the relationship between Seismic Quality Factor (Q) and Peak Ground Acceleration (PGA). Q measurements were performed from EstuNet Seismic Network data that it is composed

of 18 strong-motion and 8 weak-motion stations mainly distributed in Quaternary- and Neogene-aged units in the Eskişehir Basin. The spectral ratio technique was used for calculating the absorption Q-factor.

2. Theory and Methods

The site response is a function accounting for attenuation that includes the effect of geometrical spreading and the intrinsic and scattering quality factor. Q(f) is the quality factor which includes both anelastic absorption and scattering (Parolai, 2012).

2.1. Spectral Ratio Method

The Standard Spectral Ratio technique (SSR) of earthquake recording involves comparing records at nearby sites using one site as the bedrock reference site (Figure 1) (Parolai, 2012). SSR, a reference site technique, involves considering the spectral ratio of the same component of strong ground motions recorded at two nearby stations. The SSR technique was initiated by (Borcherdt, 1970). In Borcherdt (1970)'s study, ground motion generated by nuclear explosions in Nevada were measured at 37 locations near San Francisco Bay, California. These results were compared with those of the San Francisco earthquake of 1906. This technique has previously been used in many geological environments (Borcherdt, 1989; Field et al., 1992; Gök et al., 2014; Mittal et al., 2015; Özer, 2019).

The assumption of this technique is that the two sites have a similar source and path effects. If the separation between the stations' input and output is much less than their hypocentral distances from the source, it is probably a good assumption that the path terms will cancel. The critical assumption in these methods is that the surface- rock-site record (reference) is equivalent to the input motion at the base of the soil layers (Steidl et al., 1996).

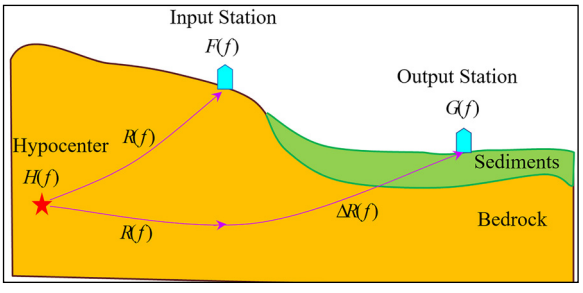


Figure 1- Typical geological structure of sedimentary basin and input-output station spectral-ratio method.

f Frequency

$H(f)$ Earthquake source function

$F(f)$ Input station function

$G(f)$ Output station function—the spectral amplitude of the ground motion observed at a recording site for an event.

$R(f)$ Path function between hypocenter and input station

$DR(f)$ Path function between input and output stations

$$F(f) = H(f)\,R(f \tag{1}$$

$$G(f) = H(f)\,R(f)\,DR(f) \tag{2}$$

$$\Delta R(f) = \frac{G(f)}{F(f)} \tag{3}$$

where H(*f*), R(*f*), ΔR(*f*) represent the spectral contribution of the source, the wavepath and local geology, respectively. At the two observation sites, with amplitude G(*f*) on sediment and amplitude F(*f*) on bedrock, the source function H(*f*) is the same (as the same signal is compared), and the wavepath function R(*f*) is also the same (with good approximation for closely located sites); whereas the local-geology function ΔR(*f*) is different (Borcherdt, 1970; Bath, 1974). Equations 1 and 2 denote input and output station functions, respectively. The path function between input and output stations is given by Equation 3 and holds if the path function between hypocenter and input station is identical to the initial part of the path function between hypocenter and output station functions. In this case, the terms H(*f*) and R(*f*) are eliminated in Equation 3.

2.2. Earthquake Wave Phases and Seismic-Q Measurements

The absorption phenomenon affects all earthquake wave phases. To measure the absorption of body waves (P- and S-waves), the analysis window should be carefully placed on the body wave arrivals. There is a problem of frequency dependence for all the component velocities of P- and S-waves, but in fact the

problem lies the more accurate interpretation (Barton, 2007). A quality factor Q-seismic was popularized by Knopoff, 1964 with the briefest possible title: Q. Generally, Q measurement methods can be classified into two main categories. In one category Q is extracted in the time domain (Engelhard, 1996). The other category comprises frequency-domain methods (Quan and Harris, 1997; Sams and Goldberg, 1990; Zhang and Ulrych, 2002). Besides, Q analysis based on amplitude attenuation and compensation functions (Wang, 2004). Estimations of the quality, Q, factor are commonly obtained from vertical seismic data or stacked surface seismic data and many techniques for estimating Q have been proposed (Bano, 1996; Dasgupta and Clark, 1998; De Castro Nunes et al., 2011; Blias, 2012; Yang et al., 2014)

In this study, the absorption measurements of surface waves were only considered (Rayleigh and Love waves); therefore, the analysis windows can cover all the seismic wave phases, including the initial body waves. By their nature, low frequency/high amplitude surface waves occupy the low frequency band of the amplitude spectrum. Conversely, low amplitude/high frequency body waves occupy the high frequency band of the amplitude spectrum. This natural discrimination of surface waves and body waves allows us to measure the absorption of surface waves in the low frequency band of the amplitude spectrum. The time domain analysis window can embrace all phases of a seismic event, therefore there is no need to position the analysis window over only the surface waves.

2.3. Computation of Q-factor

Seismic wave attenuation expressed by the quality factor Q is another field where spectral analysis is the natural approach. Attenuation methods are naturally applicable to both body waves and surface waves (Bath, 1974). The quality factor Q is often assumed to be frequency-independent and is regarded as a constant within the seismic frequency band. Several Q models have been proposed to describe attenuation mathematically (Futterman, 1962; Kjartansson, 1979; Wang and Guo, 2004). According to Q model of Futterman (1962), if one only consider the attenuation of the amplitude spectrum of the seismic wave, the attenuation mechanism can be depicted as

$$G(f) = F(f)\, e^{-\frac{\pi t f}{Q}} = F(f)\, e^{-af} \quad (4)$$

t Travel time (s); the travelling time difference between the received waveform and the source wavelet.

Q Q-factor

a Slope (s)

f Frequency (Hz)

$F(f)$ Input station function

$G(f)$ Output station function

Based on the above attenuation mechanism, proposed to obtain Q using the spectral ratios. The spectral-ratio technique has been applied to real data but is unstable and not very reliable (Sams and Goldberg, 1990). The logarithmic spectral ratio (LSR) is frequency domain methods. This method is based on the change of spectral properties of seismic waves as they propagate through anelastic medium (Dasios et al., 2001). The LSR method uses a selected band of the Fourier frequency spectra. This phenomenon was investigated by using real data.

The slope is given as:

$$a = -\frac{\pi t}{Q} \quad (5)$$

From Equation 3, the natural logarithm of output to input functions ratio:

$$ln\,\Delta DR(f) = ln\frac{G(f)}{F(f)} = -\frac{\pi t}{Q} f = -af \quad (6)$$

The Q-factor is then given as:

$$Q = -\frac{\pi t}{a} = -\frac{\pi tf}{\ln\frac{G(f)}{F(f)}} \quad (7)$$

According to the third term of Equation 7, Q-factor can be computed for each value of the frequency *f*. However, real data values scatter around the slope segment (Figure 2), yielding to different Q-factor values. If the real data values fall on the slope segment, the same Q-factor values should be obtained. Therefore, based on the distribution of the real data, a slope segment should first be selected and then the slope value determined. The second term in the Equation 7 may be used for Q-factor computations

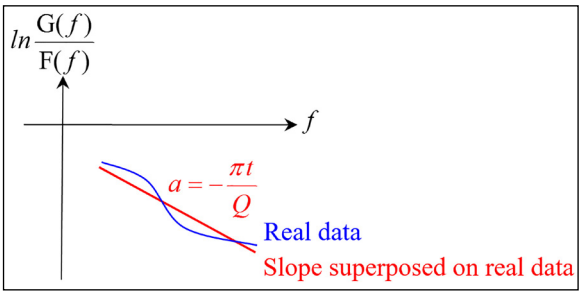


Figure 2- Measurement of slope.

eliminating the undesired effects of data scattering. The travel time *t* is a monotonically increasing variable as the seismic waves travel in space. The slope *a* in the denominator of Equation 7 is the most effective term in the determination of Q-factor. Along the travel path, inclusion and exclusion of low or high Q-value rocks severely influence the value of slope *a*. Therefore, the slope *a* should be carefully determined.

2.4. Computation of Surface Waves Q-factor from P-Waves Travel Time

Although it is easy to observe the onset times of P-waves in seismograms, the onset times of surface waves cannot be clearly determined due to the crowdedness caused by body waves prior to surface wave arrivals.

$$Q = -\frac{\pi t_R}{a} = -\frac{\pi x}{a V_R} \tag{8}$$

$$v_R = 0.92 v_S \tag{9}$$

$$\frac{V_S}{V_P} = \sqrt{\frac{0.5-\sigma}{1-\sigma}} \tag{10}$$

$$Q = -\frac{\pi x}{a V_R} = -\frac{\pi x}{a\, 0.92 V_S} = -\frac{\pi x}{a V_P 0.92\sqrt{\frac{0.5-\sigma}{1-\sigma}}} \tag{11}$$

$$Q \approx -\frac{\pi x}{a V_P 0.92\sqrt{\frac{0.5-0.26}{1-0.26}}} = -\frac{6x}{a V_P} = -\frac{6 t_P}{a} \tag{12}$$

In Equation 8, t_R denotes the travel time of surface waves, *a* is the slope, *x* is the travel distance, and V_R is velocity of the fastest phase of the surface waves. Equation 9 gives the relation between surface waves and S- waves. Equation 10 represents Poisson's ratio. Equation 11 is obtained from the substitution of Equations 8, 9 and 10.

In dry rocks, Poison's ratio may be taken as $\sigma = 0.26$ (Christensen, 1996). In such a case, the overall multiplier assumes the value of 6. Hence, Equation 12 can be used to obtain surface waves Q-factor from P-wave travel times t_P.

2.5. Surface Waves Dispersion and Q-factor Computation

Insertion of dispersive velocity function to Equation 4 yields:

$$G(f) = F(f)\, e^{-\frac{\pi t}{Q} f}\, e^{-i\frac{2\pi x}{V(f)} f} \tag{13}$$

In Equation 13, output *G(f)* and input *F(f)* are complex functions where *i* denotes the imaginary term and *V(f)* is the dispersive velocity function. The computation of Q-factor is performed on the real function $exp(-\pi tf/Q)$ only. Therefore, computation of Q-factor is not affected by the imaginary function $exp(-i2\pi xf/V(f))$. When positioning the time analysis window over the seismogram, all wave trains related to surface waves should be included in the computations.

3. EstuNet Seismic Network and Geological Structure

The establishment of the EstuNet Seismic Network and operation studies first began in 2005 with the creation of 5 stations, which subsequently increased to 21 with the support of two Anadolu University Research Projects (Figure 3). Thirteen of the stations are strong motion; eight are weak motion.

All stations were free-field and equipped with the CMG-5TD, three-axis strong-motion accelerometer, a 24-bit digitizer, and a flexible data acquisition and storage unit packaged together in a single sealed case. The systems contain two supply boxes with ADSL, GPRS, a satellite modem for communication, and uninterruptible power (Figure 4). Since 2015, EstuNet Seismic Network comprises 13 accelerometers spatially distributed in Eskişehir basin to represent the behaviors of different sediment thickness and different geologic formations of the half-graben structured basin (Figure 5). Stations are also located near active fault segments. The location of the accelerometer stations was chosen according to faults, local soil conditions, and settlement density. The parameters of the stations were given in Table 1.

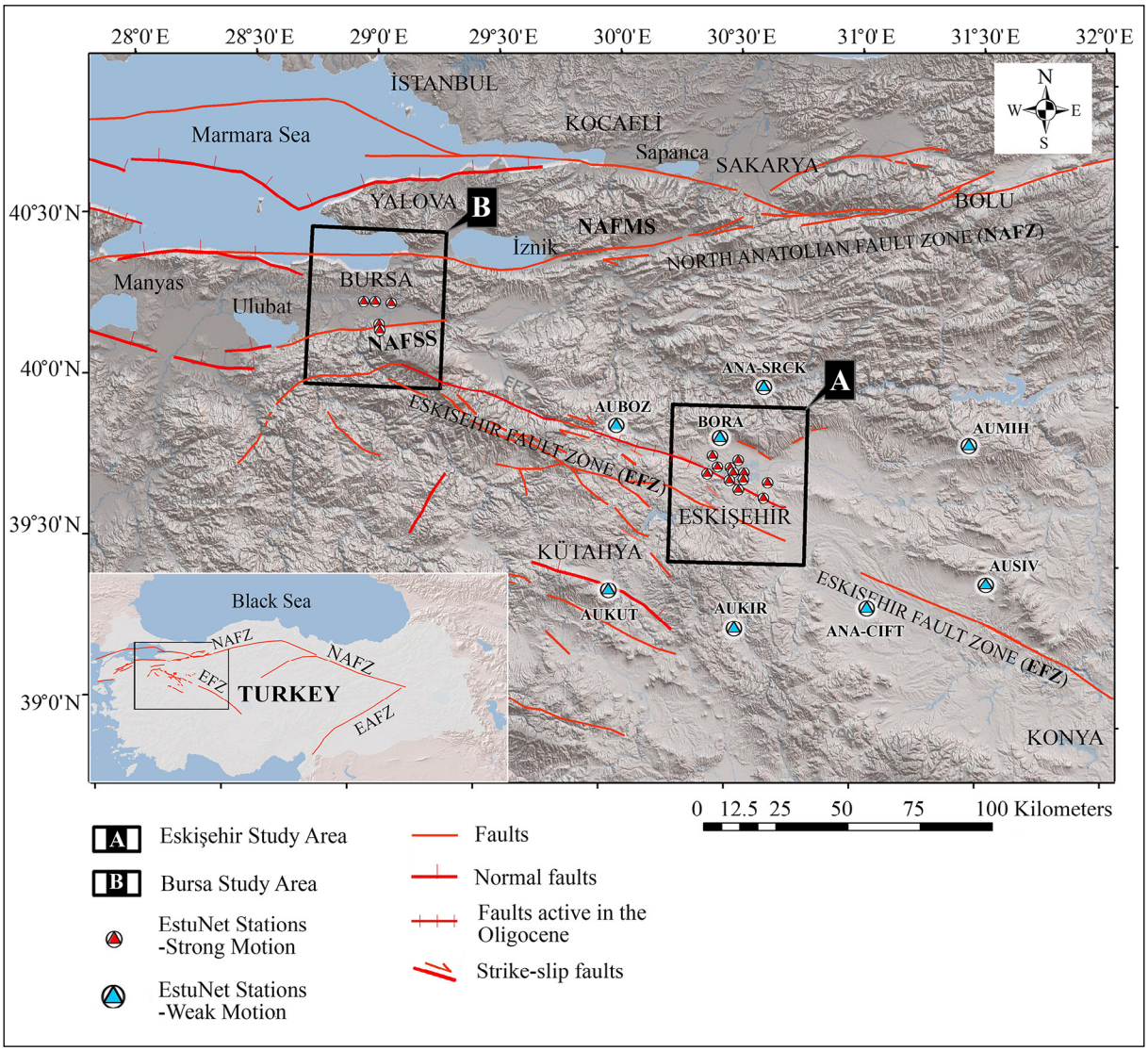


Figure 3- Regional map showing the active faults in Western Anatolia, Turkey (modified from Şaroğlu et al., 1992; Emre et al., 2013) and the location of EstuNet Seismic Network stations. NAFZ-North Anatolian Fault Zone, NAFMS-middle strand of North Anatolian Fault, NAFSS- southern branch of the North Anatolian Fault, EFZ- Eskişehir Fault Zone, EAFZ-East Anatolian Fault Zone, EG-Eskişehir Graben.

4. Implementation: M= 4.3 Eskişehir 17.01.2015 Earthquake

The dataset considered in this study includes the strong ground motion data of the 2015 Alınca, Eskişehir earthquake. The Alınca, Eskişehir earthquake of January 17, 2015, magnitude 4.3, was thought to have taken place in the Alınca segment, located northwest of the Eskişehir basin at a depth of 5.5 km (from KOERI). Identified as having a normal fault, the earthquake was recorded by 11 strong motion stations of the EstuNet Seismic Network. Table 2 reports these records, which show the arrival time of the earthquake from the epicenter to the stations, and the peak ground acceleration values. Distance values reported in Table 2 refer to the distance between the accelerometer station and the epicenter of the earthquake. The first row in Table 2 (bold typeface) reports records from the nearest station. The other rows report records from further stations.

In Figure 6, the components for each station are arranged with the vertical component at the top in red and the two horizontal components below. The N-S component is shown in blue and E-W component in green (Figure 6a). Fourier transformations were

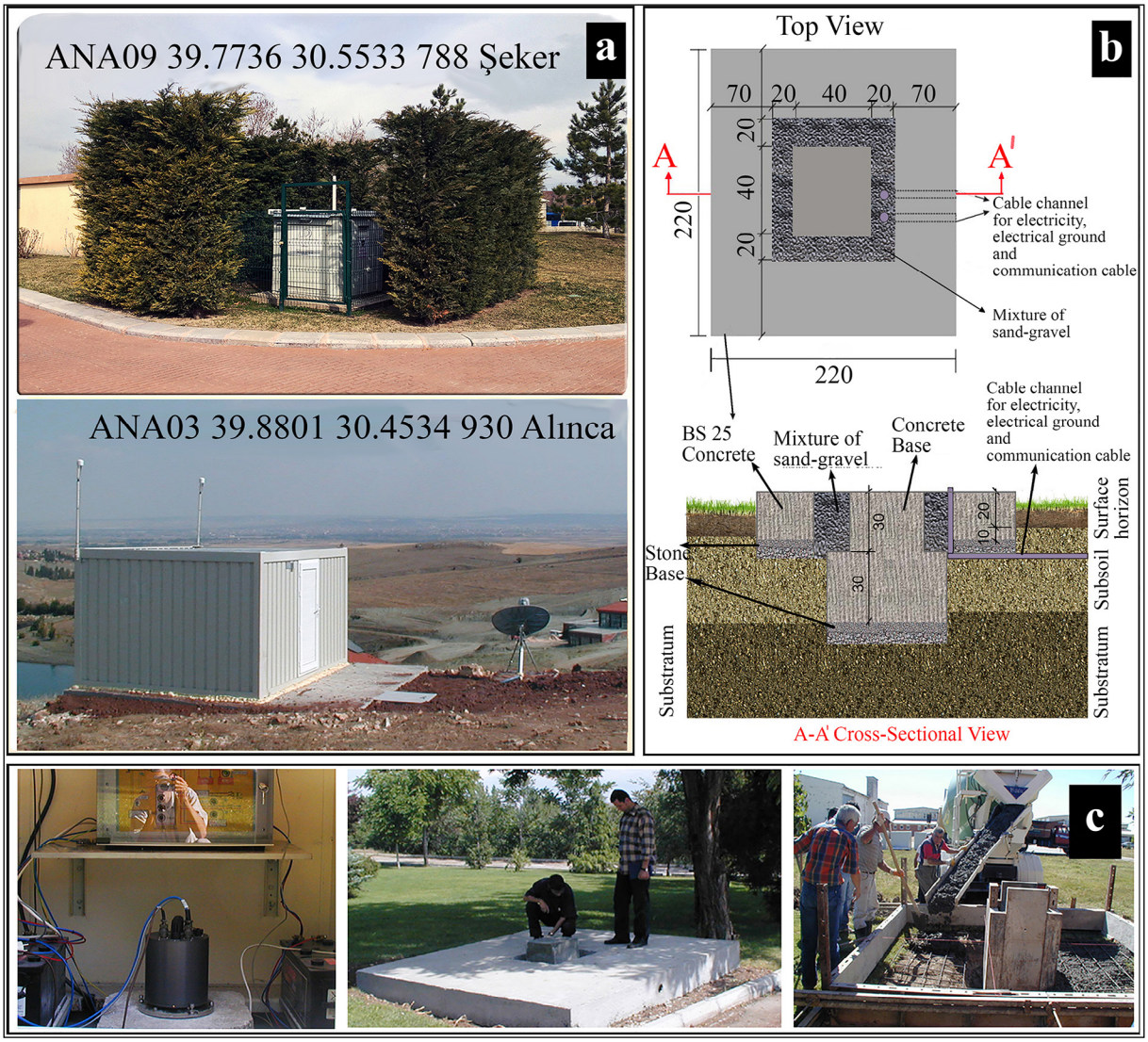


Figure 4- Typical installation of EstuNet strong/weak-motion network; a) recording stations are cabined in the standardized small galvanized hut as shown at ANA09, OSG5 locations, b) infrastructure of strong-motion stations is built according to the schema, c) pictures of the stages of construction, inner view of a container with a typical installation of free-field station, Guralp CMG-5TCDE built-in system mounted on a concrete base (modified from Tün et al., 2020).

calculated for each of the records, taking the frequency upper limit into consideration; amplitude spectrum curves were drawn (Figure 6b). The amplitude spectrum curves provide information on which station to use as the reference (the station in denominator of the ratio). ANA03 station (curves with a light color) is the best candidate to use as the reference, as it is the closest to the focus of the earthquake (data that are rich in terms of frequency content) and it contains no alluvial deposit (data that have no resonance effects). The amplitude spectrum curves of the reference station should be as straight as possible (ie, should contain few peaks) and have a large frequency band in order to detect anomalies such as site fundamental periods in the other stations with which it is compared (the station in the numerator of the ratio). Because data are from the same earthquake, the source functions are the same. Thus, the ratios can serve as indicators of ground differences between the two stations. The analysis windows cover all seismic wave phases, including the initial body waves. Their spectra were then computed (Figure 6).

Subsequently, all the stations were divided by the reference station, ANA03. Because the curve obtained was a noisy one, it had to be smoothed before

Table 1- Stations parameters AnaNet strong motion network.

No	STATION CODE	Lat. Deg N	Lon. Deg E	Elev. (m)	Location	Instrument Type	Installation Date	Connection Type
1	2601 ANA01	39.8135	30.5284	787	İki Eylül Campus	Guralp 5TCDE	07.12.2005	Local Network
2	2602 ANA02	39.7893	30.4972	815	Yeşiltepe	Guralp 5TD	14.03.2005	Local Network
3	2603 ANA03	39.8801	30.4534	930	Alınca	Guralp 5TD	09.03.2005	Satellite
4	2604 ANA04	39.7732	30.5101	770	Kırmızıtoprak	Guralp 5TCDE	09.12.2005	3G/EDGE
5	2606 ANA05	39.7488	30.4956	833	Büyükdere	Guralp 5TD	10.12.2005	ADSL
6	2610 ANA06	39.8245	30.4243	837	Yukarısöğütönü.	Guralp 5TD	14.06.2010	ADSL
7	2611 ANA07	39.7900	30.4453	813	Batıkent	Guralp 5TCDE	30.09.2014	3G/EDGE
8	2612 ANA08	39.7669	30.4049	833	Karabayır	Guralp 5TD	15.09.2012	ADSL
9	2613 ANA09	39.7736	30.5533	788	Şeker	Guralp 5TD	07.09.2012	ADSL
10	2614 ANA10	39.7529	30.5521	860	Erenköy	Guralp 5TD	08.09.2012	ADSL
11	2615 ANA11	39.7443	30.6503	814	Organized Industry	Guralp 5TD	14.06.2010	3G/EDGE
12	2616 ANA12	39.6974	30.6346	916	Sultandere	Guralp 5TD	15.06.2010	ADSL
13	2617 ANA13	39.7211	30.5326	936	Asrı Cemetery	Guralp 5TCDE	11.09.2012	3G/EDGE

Lat.: latitude, Deg: degree, Long.:longitude, Elev.: elevation.

Table 2- The recording of Eskişehir earthquake, M:4.3-17.01.2015 at accelerometer stations at the AnaNet seismic network.

Station	Arrival time	Travel time *tP*(s)	Distance (km)	PGA (gal)
ANA03	**02:42:36:90**	**2.90**	**4.98**	**80.9**
ANA01	02:42:38:40	4.40	13.86	11.8
ANA02	02:42:38:55	4.55	13.72	15.7
ANA05	02:42:39:25	5.25	17.36	13.8
ANA06	02:42:37:40	3.40	7.14	49.7
ANA07	02:42:38:35	4.35	11.36	27.9
ANA08	02:42:38:70	4.70	13.11	7.80
ANA09	02:42:39:20	5.20	18.30	12.9
ANA10	02:42:39:60	5.60	19.86	2.10
ANA11	02:42:40:70	6.70	26.83	11.6
ANA12	02:42:31:15	7.15	29.19	1.90

Earthquake: 2015.01.17, ML:4.3, Depth:5.5 km.
Lat (Deg N): 39.8848, Lon (Deg E): 30.3955, Karacobanpınarı (Alınca)-Tepebaşı-Eskişehir,
Time: 02:42:34:00 (koeri.boun.edu.tr)

continuing with the analysis. The filtering effect of the moving average window lengths applied to the ratio curves of ANA12 and ANA03 stations on moving average window length.

MAWL (1, 10 and 20), E, N and Z components, is shown in Figure 7. This operation was also carried out for the other distant station records. In logarithmic ratio graphs, where the frequency upper limit is 10 Hz, fundamental frequencies of the sites are indicated by the peaks on the curves.

ANA12/ANA03 was shown in Figure 8a. The difficulty in the measurement of the Q-factor results from the need to make the calculations in a frequency environment. The calculation method requires having

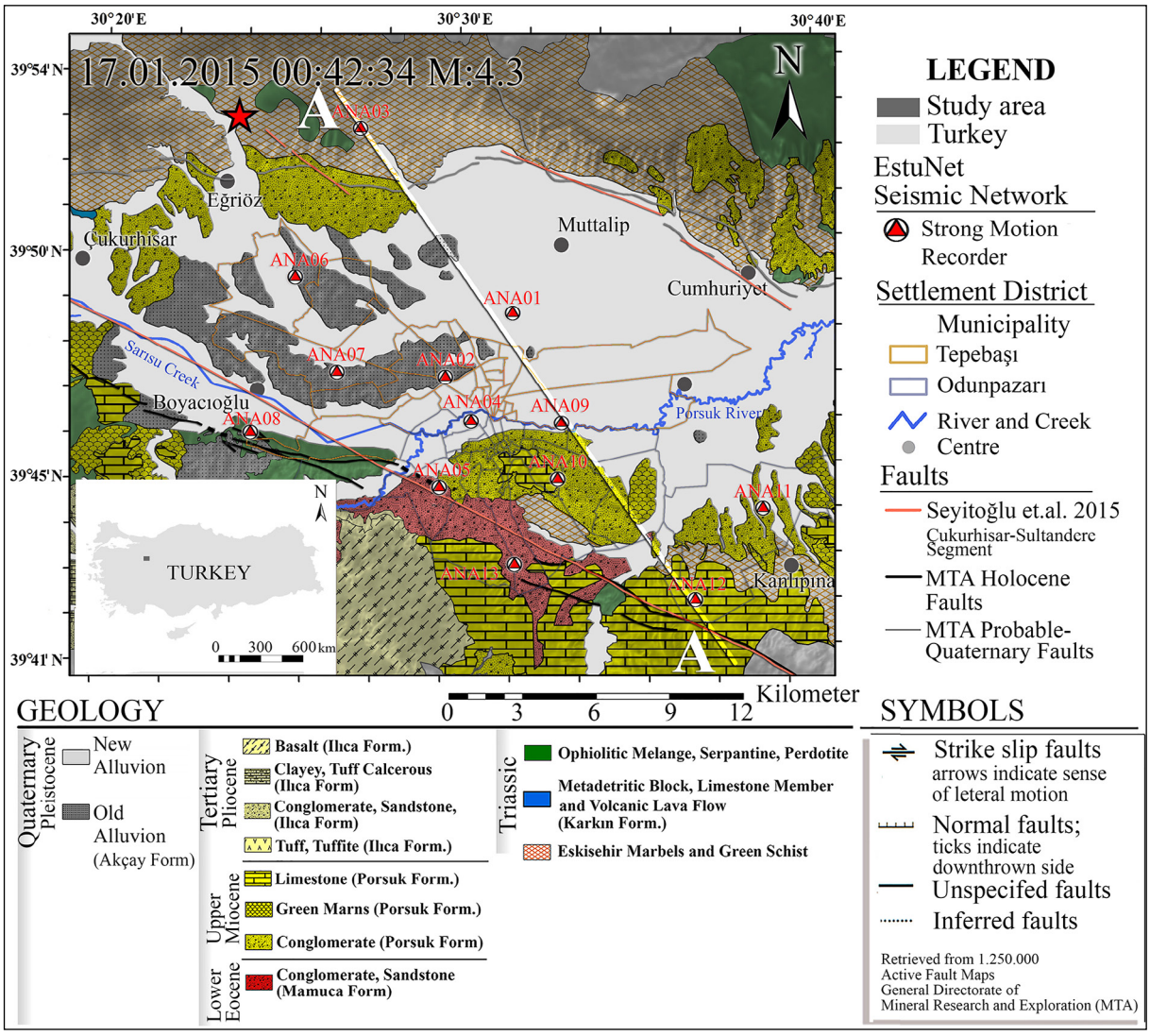


Figure 5- Regional map showing the active faults and geology in Western Anatolia, Turkey (modified from Şaroğlu et al., 1992; Orhan et al., 2007; Emre et al., 2013; Seyitoğlu et al., 2015) and the location of EstuNet seismicnNetwork stations.

the natural logarithm of the amplitude spectrum ratios of earthquake data collected from both close and distant stations. The Q-factor is calculated using the slope of a line segment (Figure 8b) located on the obtained curve. In this study, Q- factor was calculated using Equation 12. In this equation, *t* refers to the travel time for P-waves to travel between close and distant stations, and *a* refers to the slope value obtained in the spectral environment. Figure 9 displays close/distant and ln(close/distant) station data recorded by ANA03 and ANA12 stations for the M4.3 Alınca earthquake. Q values from these data were calculated by solving Equation 12 using the slopes of the line segments placed on ln(close/distant) curves and the differences in travel times between close and distant stations, as shown in Table 2.

5. Findings and Discussion

For each accelerometer station, PGA values reported in Table 2 and Q values, calculated by using ANA03 as the reference station, were compared (Figure 9). The figure shows the peak acceleration values calculated for each station on the left vertical axis and the quality factor values calculated on the right vertical axis. The first issue to note in this graph is the inverse relationship between Q values and PGA values, depending on the distance between the source

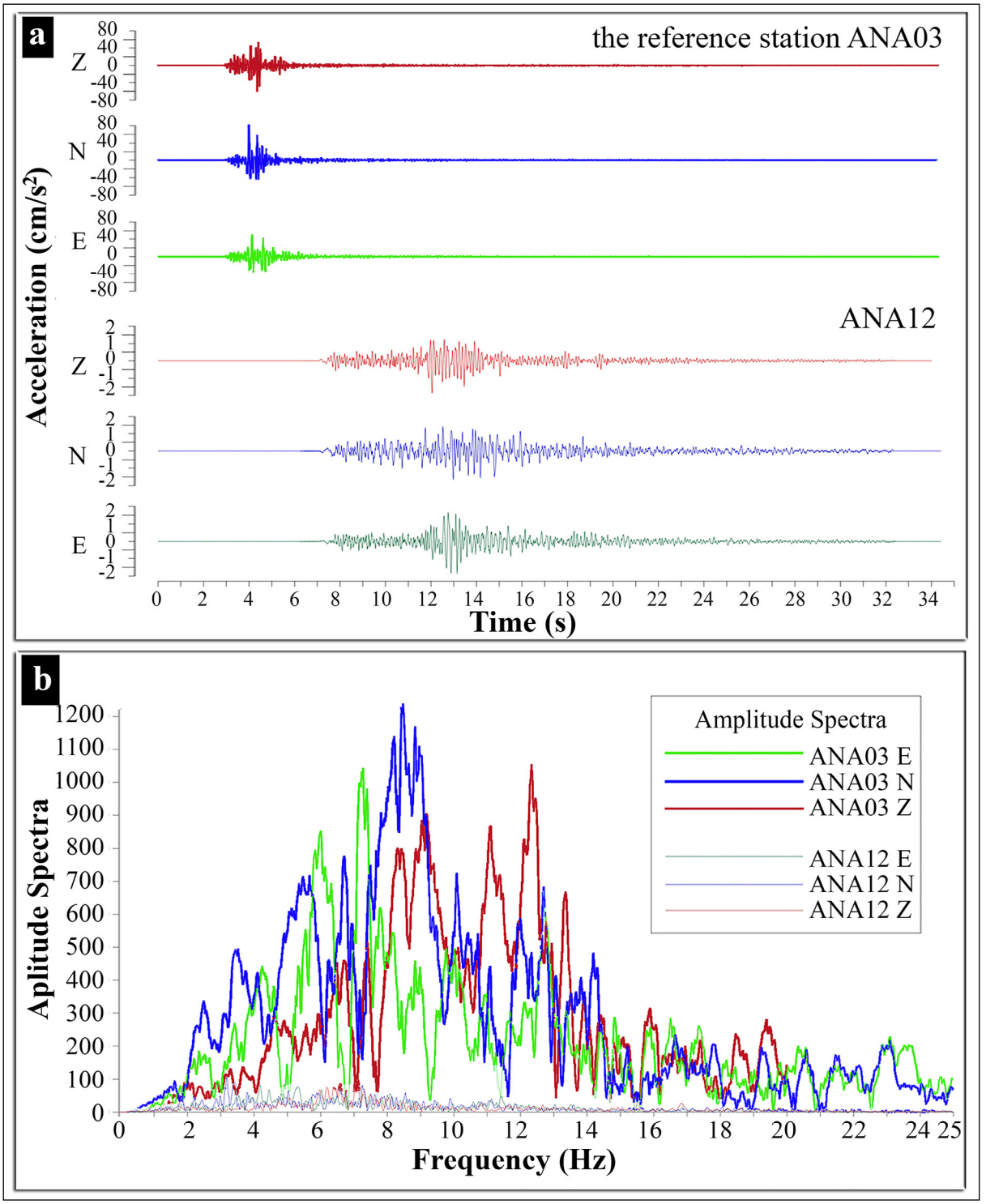


Figure 6- a) The time histories of accelerations recorded at Eskişehir Basin from the ML 4.3, 17 January 2015, Alınca Segment, Eskişehir earthquake, b) computed amplitude spectra curves.

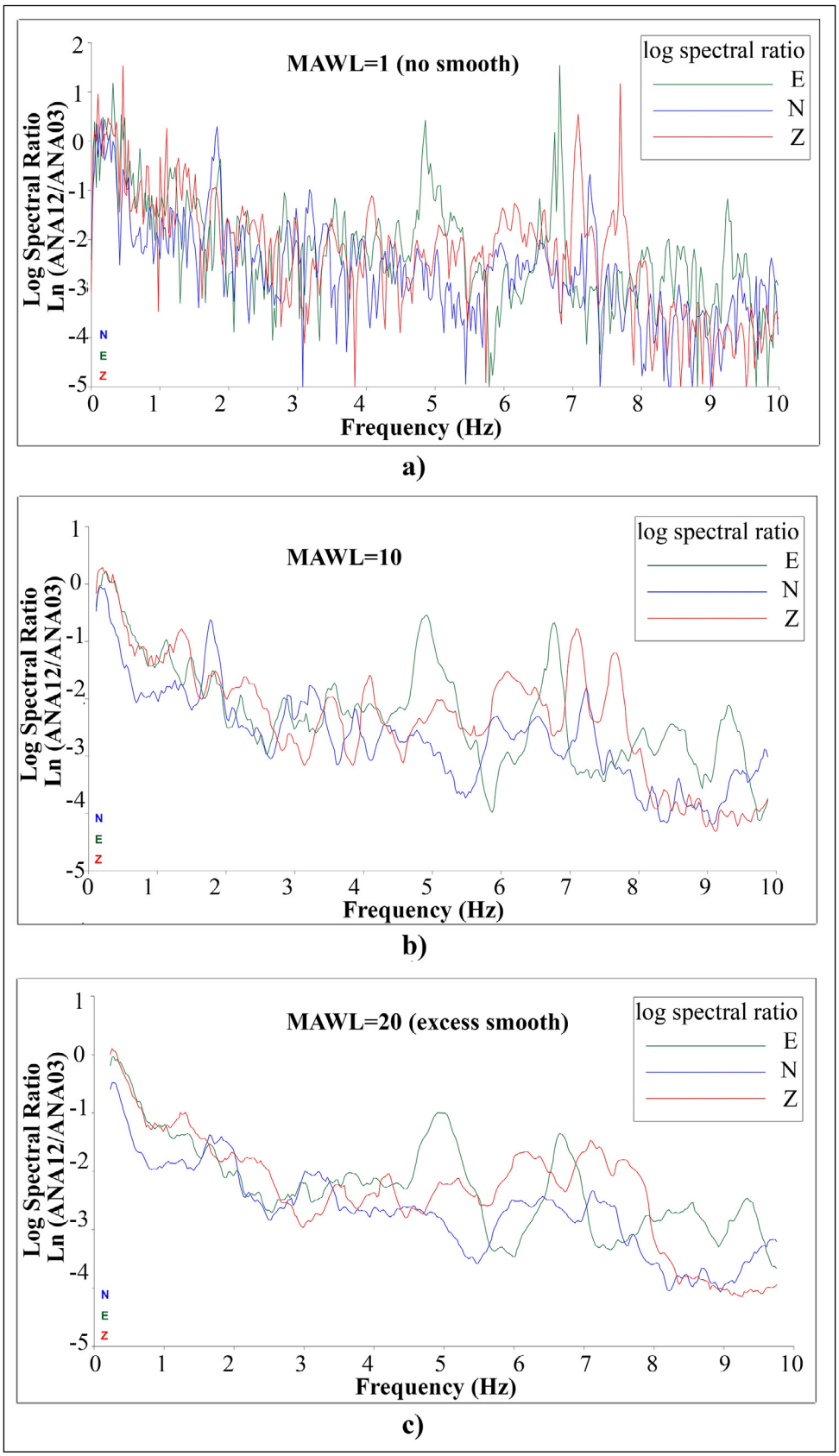


Figure 7- The filter effect results from moving average window length MAWL=1, 10, 20 for Ln(ANA12/ANA03).

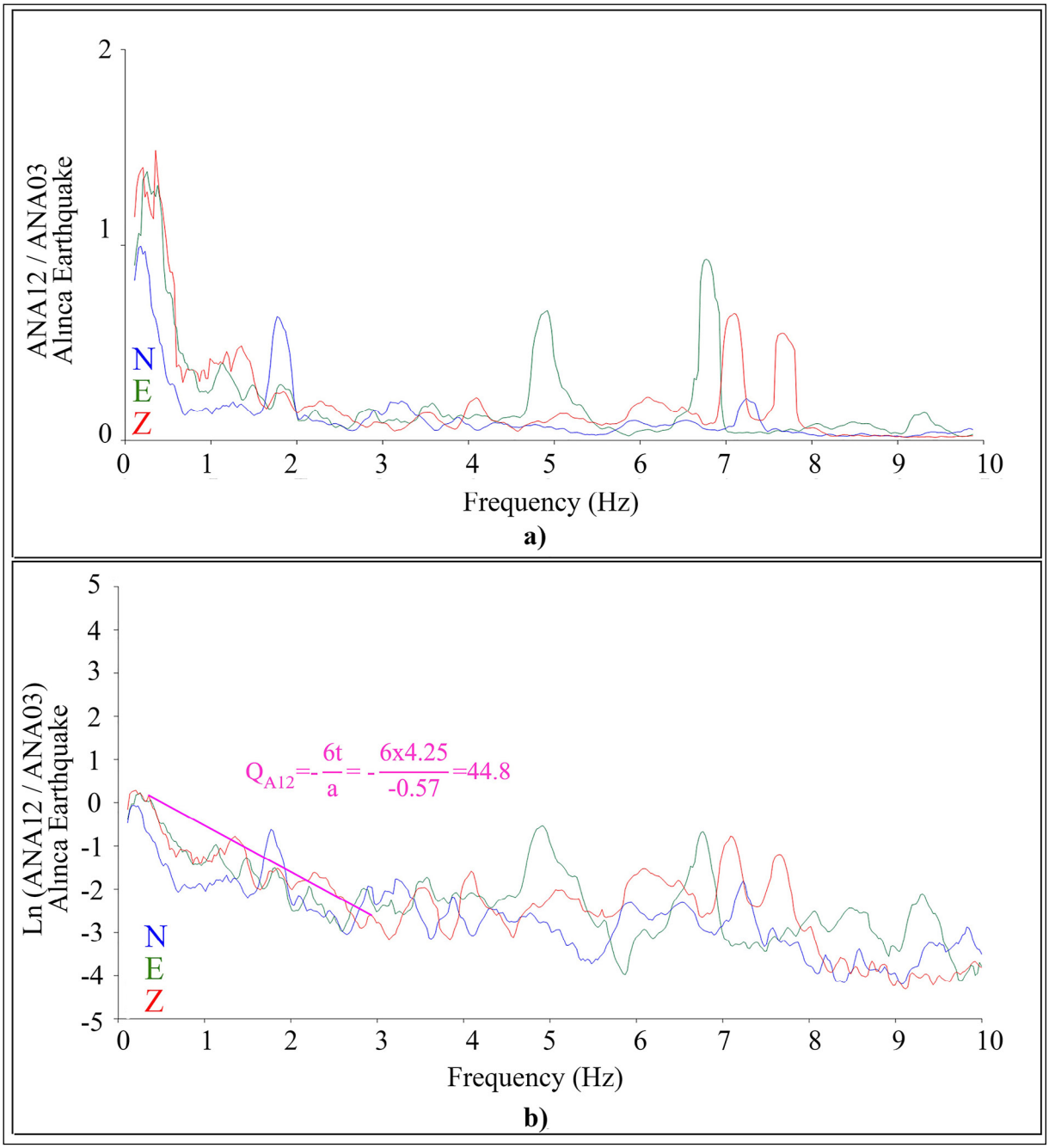


Figure 8- The calculation of quality factor Q in the Alınca Earthquake M= 4,3; a) spectral ratio: ANA12/ANA03; b) ln(ANA12/ANA03) and quality factor were calculated by Equation 12. Blue is N-S, green is E-W, and red is the vertical components. Q was calculated from the slope of the purple curve belonging to ANA03 and ANA12.

and the station. Peak ground acceleration values are known to decrease depending on the attenuation of the earthquake waves and vary by local ground conditions. High PGA values observed may be attributed to proximity to the source of the earthquake or to low quality factors. In addition, the observation that stations with high quality factors had lower peak acceleration values can be attributed to high Q values decreasing surface tremor.

For the Q-factor on the seismic wave route to remain constant, the *t/a* ratio must remain constant. Assuming that this ratio remains constant, an increase in *t* causes a proportional increase in *a*, which is the slope of the Ln|Y(f)/U(f)| curve. Equation 12 shows that *a* varies

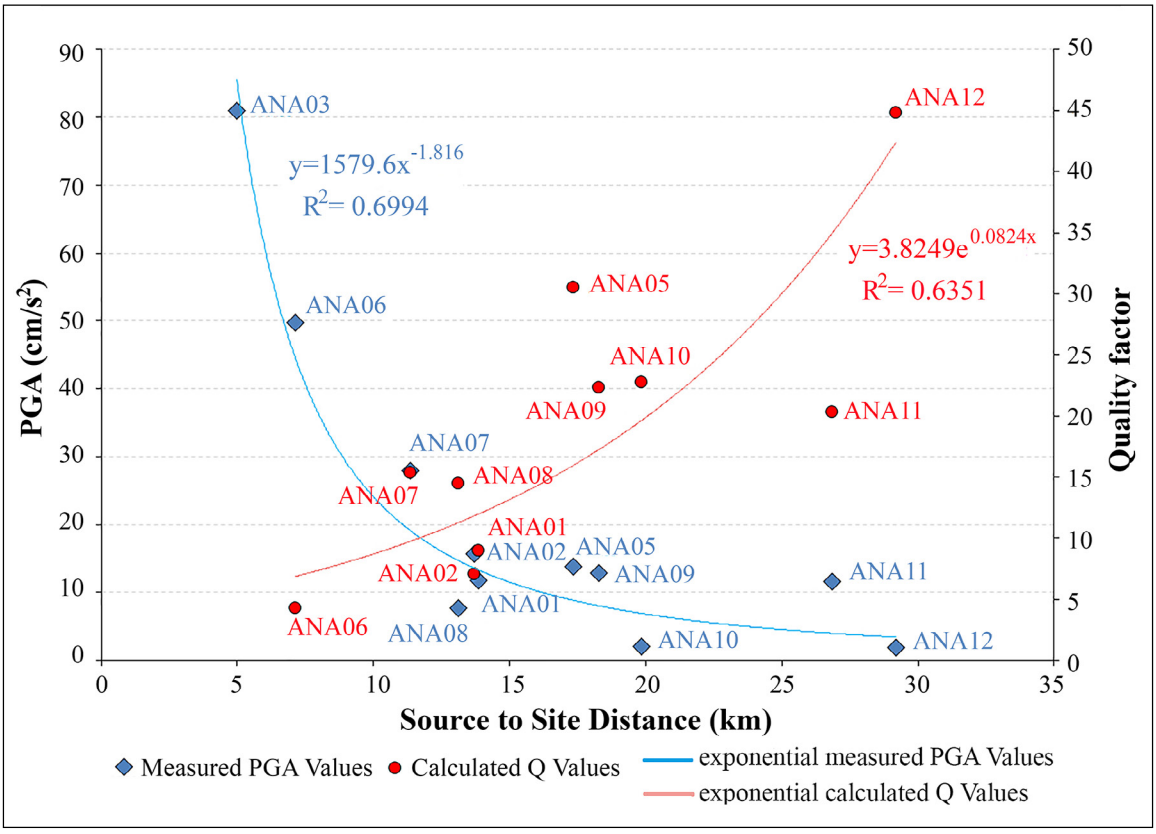


Figure 9- Blue denotes observed PGAs; red is calculated Q-factor for Alınca Earthquake ML:4.3 in the Eskişehir basin.

as the seismic quality of the rocks on the seismic wave route changes. When the seismic quality of the rocks on this route decreases (when average Q decreases), *a* is observed to increase. When the seismic quality of the rocks increases (when average Q increases), *a* is observed to decrease. As the seismic wave proceeds, *t* constantly increases, but *a* is observed to increase or decrease, depending on the seismic quality of the rocks on the route.

As can be seen in Figure 10, for the Q value calculated as 9.0 for the route between ANA03 (close) and ANA01 (distant) stations to remain the same on the route between ANA03 (close) and ANA12 (distant) stations, the slope at ANA12 station would have to be a=-6×t/Q=-6×4.25/9.0=-2.83 s. The actual slope measured at ANA12 station, however, is a=-0.57 s. This decrease in the slope shows that there are rocks with higher seismic quality on the route between ANA03 and ANA12 stations (Q=44.8). If there were rocks with a lower seismic quality on this route, the slope would have been 'a<-2.83 s' (Q<9.0).

The geological and tectonic model through the A-A' cross-section shown in Figure 5 was built using previous studies. To this end, horizontal-to-vertical spectral ratio (HVSR) measurements previously conducted in the region were used and bedrock depth through the A-A' cross-section was estimated. The HVSR method calculates the spectral ratio of the horizontal component to the vertical component (Kanai et al., 1954). These studies show that peaks in the HVSR curves result from a large impedance contrast between the soft sediments and the bedrock. The relationship between the top sediment thickness and the fundamental resonance frequency (fr) values was studied (Tün, 2013). The relationship of fundamental frequency and bedrock depth is a simplified representation without considering the complexities of shallow subsurface structure. A section of the basin was taken along a NW-SE diagonal in order to be able to see the half-graben structure and the compatibility of the graben geometry with the existing faults (Figure 11). As Figure 12b shows, the Q value calculated for ANA12 station, located on limestone, is 44.8. Peak acceleration value which was measured as 80.9 gal at

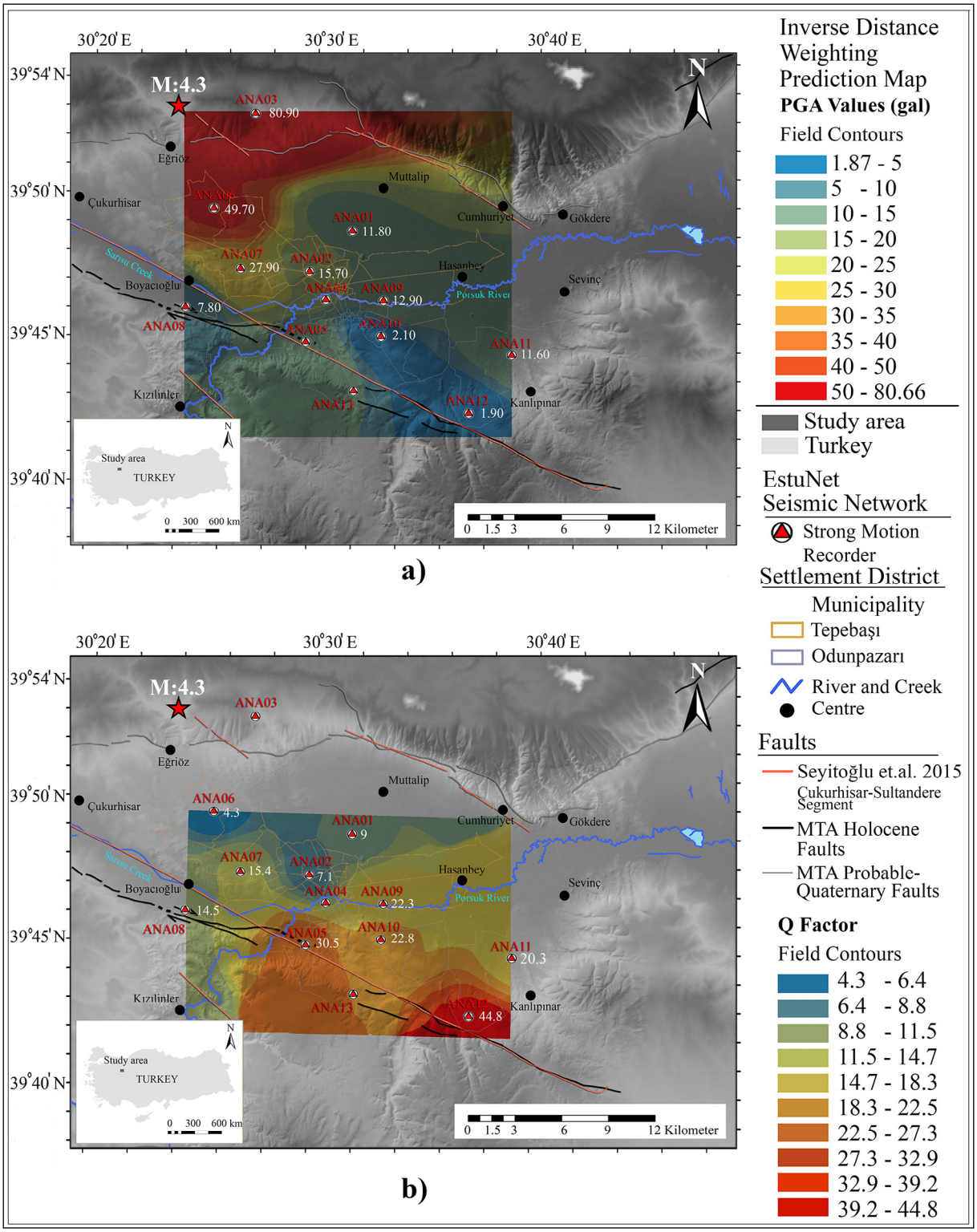


Figure 10- a) Map of PGA values for the ML 4.3, 17 January 2015, Alınca Segment, Eskişehir, earthquake, b) map of Q values for the Alınca, Eskişehir earthquake.

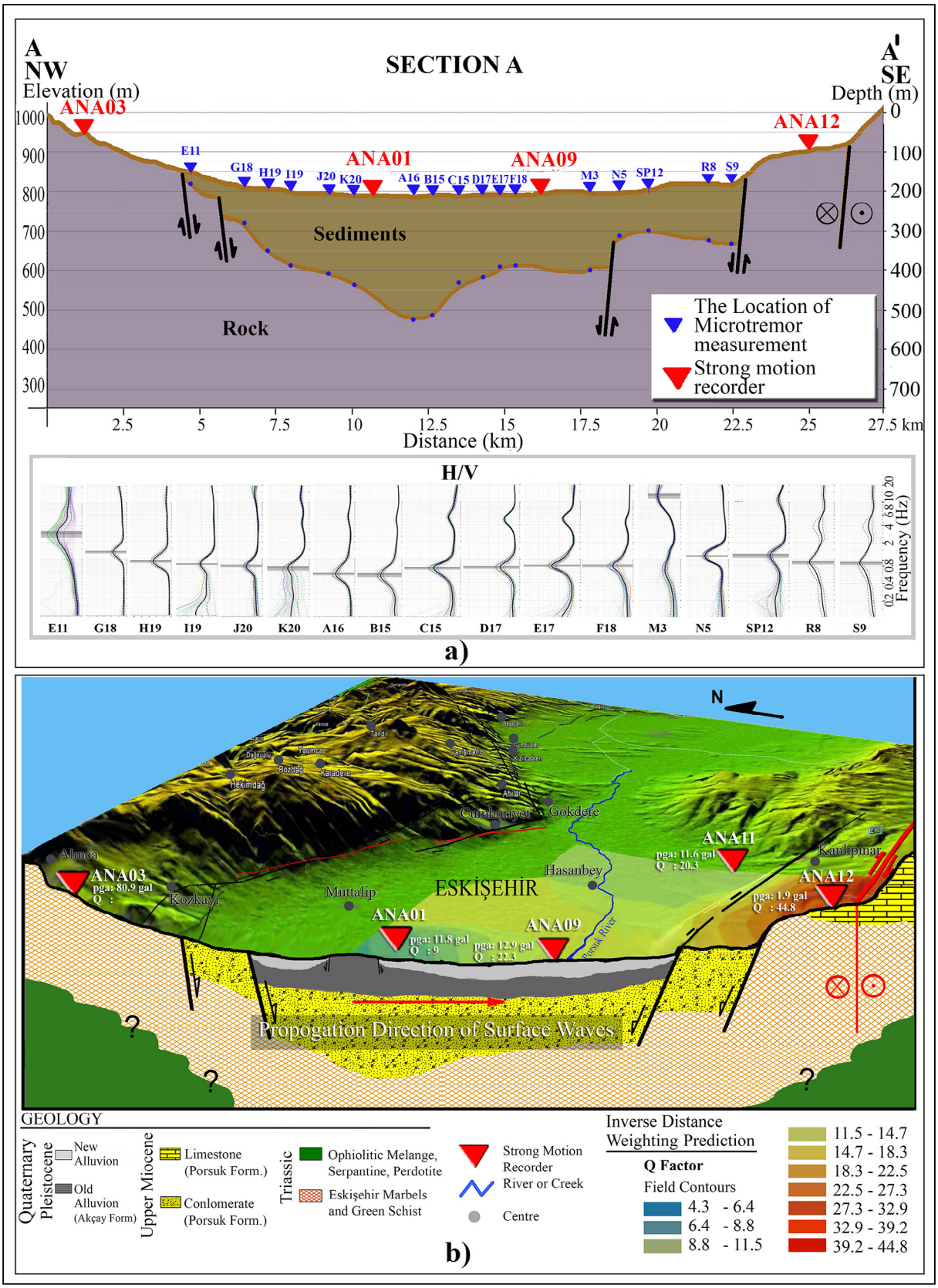


Figure 11- a) The locations of the selected HVSR curves (blue inverted triangles) and strong motion stations are projected on topography and the approximate bedrock depth along the A-A' profile, b) generalized geologic and tectonic model within the study area.

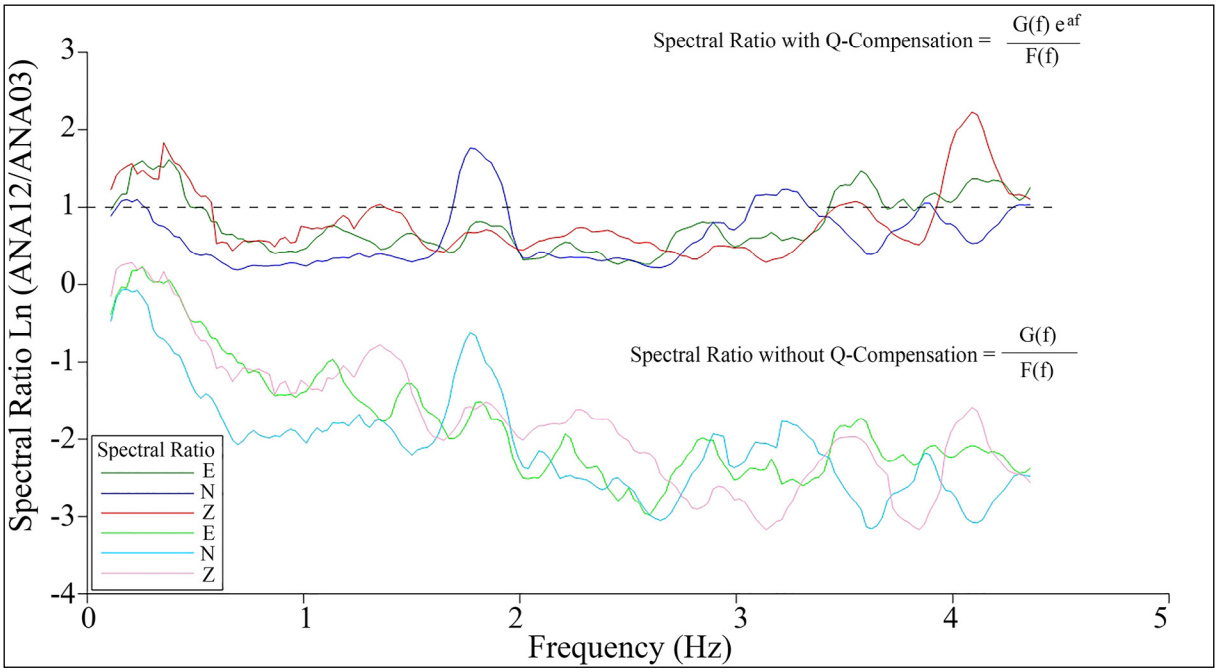


Figure 12- Removal of absorption: Q-compensation.

ANA03, the closest station to the source, decreased to 1.9 gal at ANA12 station, which is located on a bedrock segment with a high seismic quality factor. On the other hand, the peak acceleration value measured at the ANA01 station, which has a seismic quality factor of 9, was 11.6 gal.

5.1. Removal of Absorption: Q-Compensation

A Q-factor compensation process to the ln (output/input) curve was added to remove the absorption effect so that the transfer function of the earthquake waves and soil interaction can be independently analyzed.

The absorption of the seismic waves and their interaction with subsurface layers are both frequency-dependent phenomena. Both events simultaneously influence seismic waves. It was demonstrated in this study that it is possible to discern the absorption process from an interaction with layers (Figure 12).

6. Results

The contributions of this study are as follows: (1) the relationship between the computed Q-factor and measured Peak Ground Acceleration values was established; (2) an empirical formula to relate surface waves travel time t_R to P-waves travel time t_P was derived; (3) an analytical expression to prove that Q-factor computation is not affected by surface wave dispersion was derived; (4) the Q compensation step to improve the earthquake waves and soil response curves was proposed.

In this study, the quality factor in sediments was derived from the recordings of strong ground motion for frequencies ranging mainly from 1 to 5 Hz. The measured quality factor ranges between 5 and 45 in the Eskişehir Basin. The comparisons between Q values and PGA values also show good agreement. When Q-factor values are high, PGA values are low and vice-versa. Therefore, the sites where the Q factor is very low should be analyzed in more detail in ground-based earthquake risk assessments.

These basin effects, identified in the cross-section A in Figure 12, should be complemented with findings from further studies on the amplification effects of current sediment deposits, sediment thickness, velocity, and three dimensional geometry of the bedrock depth in the region.

Acknowledgements

This work was supported by the Anadolu University Research Fund under Project Numbers 1705F255. I

would like to thank Prof. Dr. Berkan ECEVİTOĞLU (Eskişehir Technical University, Eskişehir) for sharing with us his experience related to seismic interpretation.

References

Anderson, D. L., Archambeau, C. B. 1964. The anelasticity of the earth. Journal of Geophysical Research 69(10), 2071- 2084.

Anderson, D. L., Kovach, R. L. 1964. Attenuation in the mantle and rigidity of the core from multiply reflected core phases. Proceedings of the National Academy of Sciences 51(2), 168-172.

Anderson, D. L., Hart, R. 1978. Q of the Earth. Journal of Geophysical Research: Solid Earth 83(B12), 5869-5882.

Bano, M. 1996. Q-phase compensation of seismic records in the frequency domain. Bulletin of the Seismological Society of America 86(4), 1179-1186.

Bath, M. 1974. Spectral Analysis in Geophysics: Elsevier Science Publication Cooperation, Amsterdam.

Barton, N. 2007. Rock Quality, Seismic Velocity, Attenuation and Anisotropy. CRC Press, 721.

Borcherdt, R. D. 1970. Effects of local geology on ground motion near San Francisco Bay. Bulletin of the Seismological Society of America 60, 29-61.

Borcherdt, R. D. 1989. Results and data from seismologic and geologic studies following earthquakes of December 7, 1988, near Spitak, Armenia SSR (No. 89-163-A). US Geological Survey.

Blias, E. 2012. Accurate interval Q-factor estimation from VSP data. Geophysics 77(3), WA149-WA156.

Christensen, N. I. 1996. Poisson's ratio and crustal seismology. Journal of Geophysical Research Solid Earth 101, 3139-3156.

Dasgupta, R., Clark, R. A., 1998. Estimation of Q from surface seismic reflection data. Geophysics 63(6), 2120-2128.

Dasios, A., Astin, McCann, T. C. 2001. Compressional-wave Q estimation from fullwaveform sonic data. Geophysical Prospecting 49(3), 353-373.

De Castro Nunes, B. I., De Medeiros, W. E., Do Nascimento, A. F., Moreira, J. A. M. 2011. Estimating quality factor from surface seismic data: a comparison of current approaches. Journal of Applied Geophysics 75(2), 161-170.

Emre, Ö., Duman, T., Özalp, S., Elmacı, H., Olgun, Ş., Şaroğlu, F. 2013. Active fault map of Turkey with explanatory text. General Directorate of Mineral Research and Exploration, Special Publication Series 30, Ankara, Turkey.

Engelhard, L. 1996. Determination of seismic-wave attenuation by complex trace analysis. Geophysical Journal International 125(2), 608-622.

Ersoy, İ. 1956. Eskişehir Depremi, ARKİTEKT, 74-75.

Field, E., Jacob, K., Hough, S. 1992. Earthquake site response estimation: a weak-motion case study, Bulletin of the Seismological Society of America 82, 2283-2307.

Futterman, W. I. 1962. Dispersive body waves. Journal of Geophysical Research 67(13), 5279-5291.

Gok, E., Chávez-García, F.J., Polat, O. 2014. Effect of soil conditions on predicted ground motion: Case study from Western Anatolia, Turkey. Physics of the Earth and Planetary Interiors 229, 88-97.

Gurevich, B., Pevzner, R. 2015. How frequency dependency of Q affects spectral ratio estimates. Geophysics 80, A39- A44.

Jackson, D. D., Anderson, D. L. 1970. Physical mechanisms of seismic-wave attenuation. Reviews of Geophysics 8(1), 1-63.

Johnston, D. H., Toksöz, M., Timur, A. 1979. Attenuation of seismic waves in dry and saturated rocks: II. Mechanisms. Geophysics 44, 691-711.

Jongmans, D. 1990. In-situ attenuation measurements in soils, Engineering Geology 29, 99-118.

Kanai, K., Tanaka, T., Osada, K. 1954. Measurement of the microtremor I, Bulletin of the Earthquake Research Institute of Tokyo 32, 199-209.

Kjartansson, E. 1979. Constant Q-wave propagation and attenuation. Journal of Geophysical Research: Solid Earth 84(B9), 4737-4748.

Knopoff, L. 1964. Department of Physics and Institute of Geophysics and Planetary Physics University of California, Los Angeles. Reviews of Geophysics 2(4), 625-660.

Li, J., Wang, S., Yang, D., Dong, C., Tao, Y., Zhou, Y. 2016. An improved Q estimation approach: the weighted centroid frequency shift method. Journal of Geophysics and Engineering 13(3), 399.

Luzi, L., D'Amico, M., Massa, M., Puglia, R. 2019. Site effects observed in the Norcia intermountain basin (Central Italy) exploiting a 20-year monitoring. Bulletin of Earthquake Engineering 17, 97-118.

Mayoral, J., Asimaki, D., Tepalcapa, S., Wood, C., Roman-de la Sancha, A., Hutchinson, T., Franke, K., Montalva, G. 2019. Site effects in Mexico City basin: past and present. Soil Dynamics and Earthquake Engineering 121, 369-382.

Mittal, H., Kumar, A., Kumar, R. 2015. Analysis of ground motion in Delhi from earthquakes recorded by strong motion network, Arabian Journal of Geosciences 8, 2005-2017.

Miyakoshi, H., Tsuno, S., Chimoto, K., Yamanaka, H. 2019. Investigation of site amplification factors for S-and P-waves from spectral inversions in the Tokyo metropolitan area, Japan—for application to earthquake early warnings. Journal of Seismology 23(3), 561-578.

Moya, A., Irikura, K. 2003. Estimation of site effects and Q factor using a reference event. Bulletin of the Seismological Society of America 93, 1730-1745.

Naresh, B., Venkatesh, K., Mishra, L. K. 2019. Q-factor of the Punjab Basin. International Journal of Scientific Research and Review 7(9).

Orhan, A., Seyrek, E., Tosun, H. 2007. A probabilistic approach for earthquake hazard assessment of the Province of Eskişehir, Turkey, Natural Hazards and Earth System Science 7, 607-614.

Özer, Ç. 2019. Erzurum ve çevresinin yerel zemin etkilerinin incelenmesi. Dokuz Eylül Üniversitesi Mühendislik Fakültesi Fen ve Mühendislik Dergisi 21, 247-257.

Özmen, B. 2000. Ağustos 1999 İzmit Körfezi depreminin hasar durumu (rakamsal verilerle). Türkiye Deprem Vakfı 010-53, 132.

Parolai, S. 2012. Investigation of site response in urban areas by using earthquake data and seismic noise, New Manual of Seismological Observatory Practice 2, 1-38.

Press, F. 1964. Seismic wave attenuation in the crust. Journal of Geophysical Research 69(20), 4417-4418.

Quan, Y., Harris, J. M. 1997. Seismic attenuation tomography using the frequency shift method. Geophysics 62(3), 895- 905.

Raghukanth, S., Nadh Somala, S. 2009. Modeling of strong-motion data in northeastern India: Q, stress drop, and site amplification. Bulletin of the Seismological Society of America 99, 705-725.

Ricker, N. 1940. The form and nature of seismic waves and the structure of seismograms, Geophysics 5, 348-366.

Sams, M., Goldberg, D. 1990. The validity of Q estimates from borehole data using spectral ratios. Geophysics 55(1), 97-101.

Seyitoğlu, G., Ecevitoğlu, G. B., Kaypak, B., Güney, Y., Tün, M., Esat, K., Avdan, U., Temel, A., Çabuk, A., Telsiz, S., Aldaş, G. 2015. Determining the main strand of the Eskişehir strike-slip fault zone using subsidiary structures and seismicity: a hypothesis tested by seismic reflection studies. Turkish Journal of Earth Sciences 24, 1-20.

Shearer, P. M. 2009. Introduction to Seismology, 241-300.

Stein, S., Wysession, M. 2009. An Introduction to Seismology, Earthquakes, and Earth Structure. Blackwell Publishing, John Wiley and Sons, 515.

Steidl, J. H., Tumarkin, A. G., Archuleta, R. J. 1996. What is a reference site? Bulletin of the Seismological Society of America 86, 1733-1748.

Şaroğlu, F., Emre, Ö., Kuşcu, İ. 1992. Active fault map of Turkey with explanatory text, Mineral Research and Exploration General Directorate, Ankara, Turkey.

Tün, M. 2013. Interpretation of ground response and shear wave velocity (Vs) structure in microzonation studies: a case study in Eskişehir. PhD Thesis, İstanbul University.

Tün, M., Mutlu, S., Pekkan, E. 2020. EstuNet: A new weak/strong-motion network with Geodatabase for Metropolitan Eskişehir and Bursa, West Anatolia, Turkey. Journal of Earthquake Research 2(2), 193-208.

Wang, Y. 2004. Q analysis on reflection seismic data. Geophysical Research Letters 31(17).

Wang, Y., Guo, J. 2004. Modified Kolsky model for seismic attenuation and dispersion. Journal of Geophysics and Engineering 1(3), 187.

Yang, J., Cao, S., Yuan, D., Zhang, H., Shi, W. 2014. A new method for quality factor Q estimation: spectrum attributes method. 2014 SEG Annual Meeting.

Zhang, C., Ulrych, T. J. 2002. Estimation of quality factors from CMP records. Geophysics 67(5), 1542-1547.